Experimental validation of green wood peeling assisted by IR heating – some analytical system design considerations

Anna Dupleix*
Arts et Metiers ParisTech LaBoMaP, Rue Porte de Paris, F-71250 Cluny, France
School of Chemical Technology, Department of Forest Products Technology, Aalto University, FI-00076 Aalto, Finland
Phone: +33 (0)3 85 59 53 27
Fax: +33 (0)3 85 59 53 85

Jean-Christophe Batsale
Arts et Metiers ParisTech I2M, Esplanade des Arts et Metiers, F-33405 Talence Cedex, France

Andrzej Kusiak
Universite Bordeaux 1, I2M, Esplanade des Arts et Metiers, F-33405 Talence Cedex, France

Mark Hughes
School of Chemical Technology, Department of Forest Products Technology, Aalto University, FI-00076 Aalto, Finland

Louis, Etienne Denaud
Arts et Metiers ParisTech LaBoMaP, Rue Porte de Paris, F-71250 Cluny, France

_____
***Corresponding authors** email : anna.dupleix@ensam.eu

Abstract: Experimental results have been used to validate a 2D simulation model in order to check its reliability in predicting the heating of a green log rotating under an IR heating source. For the purpose of validation, it was assumed that this experimental situation could be described by simplified analytical solutions. This assumption has been confirmed. Knowing the thermal and physical characteristics of green wood, two methods are now available to calculate rapidly the temperature within the wood and the maximum surface temperature reached by a green log rotating under an IR heating source: (1) by numerical simulation and (2) by analytical equations which dispense with the computationally intensive finite element method. Experimental results, validated by both methods, show that an IR heating system embedded on an industrial peeling machine would not warm-up green wood to the required peeling temperature at current peeling speeds.

Keywords: Green wood, numerical model, on-line infrared heating, temperature field

Introduction

For certain species, the veneer peeling process requires the prior heating of round green wood to temperatures ranging from 30 to 90°C. This treatment is necessary to increase the deformability of wood, to reduce the severity of lathe checking in the veneers and to reduce cutting forces. This heating is usually done by immersing the logs in hot water (soaking); however the soaking currently used in industry to soften wood prior to peeling has a number of disadvantages. These include the duration of the process, water pollution, the need for sophisticated handling, stock downtimes and a loss of the cohesion and durability of the wood itself (Dupleix et al. 2011). Recent research on beech, birch and spruce (Dupleix et al. 2012b) has demonstrated that conventional soaking temperatures can be lowered to 50°C at the wood cutting plane, whilst still retaining acceptable peeling characteristics in terms of veneer quality (thickness variation, lathe check depth and distribution). As demonstrated by Grimhall and Hoel (1983) a possible alternative to the traditional log soaking employed in the manufacture of veneer, is the use of infrared radiation (IR) to heat green wood. This alternative technology would employ IR heaters, integrated into the peeling machine, to heat the round green wood before peeling in a manner similar to that of the laser heating sources used in the metal machining industry to soften the work-piece ahead of the cutting tool (Braham-Bouchnak et al. 2013, Rahman Rashid et al. 2012). IR heating could feasibly be used to heat the wood to the requited temperature because 70 to 90% of incident IR radiation is absorbed at the surface to a depth of around 0.3mm (Dupleix 2012c). Heat then penetrates by conduction within the green wood, with diffusivities (decreasing with increasing moisture content) of between 0.12 and 0.32 $mm^2.s^{-1}$ (Dupleix et al. 2012d). The choice of IR technology was also motivated by the potential ease with which IR heaters could be integrated

into peeling machines and by the power it offers, enabling the required heating temperatures to be achieved quickly, in line with the highly demanding peeling speeds (from 1 to 5 $m.s^{-1}$) in use in the industry.

Previous studies have demonstrated the ability of IR radiation to raise both the surface temperature and the temperature below the surface in green wood, either for the purpose of heating the wood (Makoviny and Zemiar 2004) or for drying it (Cserta et al. 2012). With heating source flux densities of 126 $kW.m^{-2}$, it has been shown that with IR heating it is possible to achieve surface temperatures of 50°C in green logs of beech, Douglas-fir and okoumé rotating at speeds corresponding to peeling speeds of 0.25-0.5 $m.s^{-1}$ (Coste 2005). Similar results have also been obtained in spruce logs rotating at speeds equivalent to peeling at 0.1 $m.s^{-1}$ using relatively low IR flux densities of 4-20 $kW.m^{-2}$ for the purpose of defreezing the logs (Bédard and Laganière 2009). As might be expected, the greater the input power of the IR source, the faster the target temperature of 50°C is achieved at a particular depth. However, the input power of the IR source must be limited in order to avoid overheating and eventual burning of the surface (Makoviny and Zemiar 2004, Marchal et al. 2004).

The aim of the work reported in this paper was to validate experimentally a 2D numerical model of the heating kinetics in a green wood cylinder rotating under an IR heating source. This model developed by Dupleix et al. (2012a) can predict the heating temperatures within wood and could potentially be used to set up the parameters of an IR heating system embedded on a peeling lathe. The validation consisted of comparing the surface and sub-surface temperatures, measured experimentally in green wood samples conveyed under an external IR heating source by thermocouples, with the numerically simulated curves of the heating rates. During this validation process, it has been demonstrated that simple analytical

equations can be used to compute the heating rates and the maximum temperatures achievable at the surface and below the surface.

Symbols, materials and methods

List of symbols:

a	diffusivity
α_{surf}^{anal}	analytical values of slopes
α_{surf}^{simul}	numerical values of slopes
c	specific heat
d	depth
D	bolt diameter
ΔMC	MC changes in the sample during heating
erfc	complementary error function
ε	emissivity of the wood surface
h	heat transfer coefficient
H	Heaviside function
HF	heat flux
IR	infrared
λ	thermal conductivity
m_f	mass of the sample after heating
m_i	mass of the sample before heating
m_{od}	mass of the oven-dried sample
MC	moisture content
MC_f	moisture content after heating
MC_i	moisture content before heating
n	vector normal to the boundary
q	IR source heat flux
q_{est}	estimated heat flux
q_{mes}	measured heat flux
ρ	wood density
RHFD	real heat flux density
s	peeling speed
t	time
t_h	heating time
T	bolt temperature
T_d	temperature attained at depth d
T_{ext}	IR source temperature
T_{init}	initial bolt temperature
T_{surf}	surface temperature
x	arc surf. of the log heated externally by IR

Experimental challenges: In general, it is a problem to assess the effective 'real heat flux density' (RHFD) received by the sample, which is needed as input data for the numerical simulation. The measurement of effective RHFD is not reliable, and thus RHFD was indirectly calculated from the surface temperatures, if the experimental situation could be

reduced to semi-infinite behaviour in the 2D Cartesian coordinates (shortly: semi-infinitive approach or simplified approach), which could be described by simple analytical equations. Thus, the numerical simulation of heating rates was validated by a three step process: 1) Testing the ability of the analytical equations (based on the simplified approach) to describe the IR heating of a green bolt. Then, 2) the RHFD received by the sample was determined by means of these analytical equations relying on the experimental surface temperature and on the inverse deconvolution method according to Beck et al. (1985). 3) The RHFD was integrated into the numerical simulation to compare experimental curves to those obtained by numerical calculations.

Samples: Knot free samples of wood were sawn (either quarter, rift or flat sawn) from the same freshly-cut tree into blocks having the following dimensions: 0.044 × 0.035 × 0.020 m^3 (see Fig.1 for a rift sawn sample). Four wood species were in focus: 2 hardwoods [European beech, *Fagus sylvatica* L; birch, *Betula pendula* Roth] and 2 softwoods [Douglas-fir, *Pseudotsuga menziesii* (Mull) Franco; spruce, *Picea albies* (L.) Karst].

Experiments: The green wood samples were conveyed at a speed, s, of 0.0032 $m.s^{-1}$ under an electric infrared lamp composed of a quartz tube delivering a heat flux density, q, onto a surface approx. 0.03 m wide (the gridded surface shown in Fig.1). The samples were shaped in the form of rectangular prisms because (1) it is easier to record internal temperature rises in a block in motion than in a rotating cylinder, (2) the numerical simulation has demonstrated that blocks behave in a similar manner to cylinders under the IR conditions applied in the present work. The time dependent surface temperature was recorded by a surface thermocouple, tightly stapled to the surface to minimize thermal contact resistance. Holes were drilled into the samples at a distance of 3 mm millimetres beneath the exposed tangential surface (Fig.1) to insert the thermocouples for temperature measurements within the block. A tight fit and filling the drilled holes with wood dust after inserting the

thermocouples ensured minimal heat losses and thermal contact resistance. The thermocouples were connected to a data acquisition system which recorded the temperature every second. The samples were initially in the green state and at least 3 replicate tests were performed with different samples (termed 'replicates' in Figs. 5 to 7) of each species (both sapwood and heartwood). The moisture contents (MCs) before heating MC_i and after heating MC_f, were determined gravimetrically by means of the following calculations:

$$MC_i\,(\%) = \frac{m_i\,(g) - m_{od}\,(g)}{m_{od}\,(g)} \qquad \text{(Eq. 1)}$$

$$MC_f\,(\%) = \frac{m_f\,(g) - m_{od}\,(g)}{m_{od}\,(g)} \qquad \text{(Eq. 2)}$$

Changes in MC during heating, ΔMC , were calculated:

$$\Delta MC\,(\%) = (1 - \frac{MC_f}{MC_i}) \times 100 \qquad \text{(Eq. 3)}$$

Numerical simulation: Comsol Multiphysics (Comsol Inc., Burlington, MA, USA) and MatLab (MathWorks Inc., Natick, MA, USA) were used to simulate the development of log surface and sub-surface temperatures over time (Dupleix et al. 2012a). The model meshes the log cross-section with 2D finite elements, as the heat flux in the longitudinal direction can be neglected. An external input heat flux density, q, was applied to a selected number of surface elements to simulate the rotation of the log in front of the IR source. The temperature distribution was calculated by solving the transient equation for conduction derived from Fourier's law (Eq.4).

$$\rho c \frac{\partial T}{\partial t} = \nabla(\lambda \nabla T) \qquad \text{(Eq. 4)}$$

where T is the bolt temperature (in K), ρ, the density of wood (in $kg.m^{-3}$), c, the specific heat capacity of wood (in $J.kg^{-1}.K^{-1}$) and, λ, the thermal conductivity of the wood (in $W.m^{-1}.K^{-1}$). The three latter parameters, varying with wood MC, were determined according to the empirical equations developed by Dupleix et al. (2012d). The influence of temperature on c

and λ was neglected, because a 40°C temperature increase (observed experimentally) leads to a variation in thermal characteristics between 7 and 12% according to Suleiman et al. (1999). The initial condition is given by the initial temperature of the bolt, T_{init} = 293 K. The boundary conditions at the bolt surface are defined by Eqs. 5a and b with, n, the vector normal to the boundary.

$$\begin{cases} \text{-on the arc surface } x\text{: } -\text{n.}(-\lambda\nabla\text{T}) = \varepsilon.q.H(x) & \text{(Eq. 5a)} \\ \text{-on the rest of the surface: } -\text{n.}(-\lambda\nabla T) = h\,(T - T_{ext}) & \text{(Eq. 5b)} \end{cases}$$

where H is the Heaviside function (Fig.2), ε, the emissivity of the wood surface, taken to be 0.85 (Dupleix et al. 2012a), T_{ext}, the external temperature (in K), h, the heat transfer coefficient (in $W.m^{-2}.K^{-1}$) and, q, flux density (in $W.m^{-2}$).

Analytical equations. Assumptions: (1) It is possible to utilise the simplified approach presented in Fig. 2., given the large dimension of the bolt diameter, D, compared to x, if the arc surface of the green log subjected to external infrared heating (x = D/20). (2) In view of the very low thermal diffusivity of green wood (Dupleix et al. 2012d), the behaviour can be assumed to be that of a semi-infinite body with a spatially uniform step heat flux diffusing normal to the surface, x, applied during a heating time, t_h, where t_h = x/s and s is the peeling speed (i.e. the constant linear speed at which veneer is generated at the output of the peeling lathe). The problem therefore becomes analogous to a 1D-transient problem where the spatial variable, x, is replaced by the temporal variable t_h. With these assumptions, the evolution of the sample surface temperature, T_{surf} , with the square root of time is linear according to Eq. 6 (Taler and Duda 2006):

$$T_{surf} = \frac{2q}{\sqrt{\pi}\sqrt{\lambda\rho c}}\sqrt{\frac{x}{s}} \quad \text{or} \quad T_{surf} = \frac{2q}{\sqrt{\pi}\sqrt{\lambda\rho c}}\sqrt{t} \qquad \text{(Eq. 6)}$$

The exact solution of the temperature, T_d , attained at depth, d, within the sample is then given by Eq. 7 [with the diffusivity of wood, $a = \lambda/(\rho c)$] (Taler and Duda 2006).

$$T_d = \frac{2q}{\sqrt{\pi}\sqrt{\lambda\rho c}} e^{-d^2/4at} \sqrt{t} - \frac{d}{\lambda} q \, \mathrm{erfc} \frac{d}{2\sqrt{at}} \qquad \text{(Eq. 7)}$$

where erfc is the complementary error function which tends to 1, when time tends to infinity. Therefore, the long-term behaviour of T_d is given by the asymptotic solution obtained when time tends to infinity (Eq.8). It can be seen that at extended heating times the temperature at depth, d, also evolves at a rate proportional to the square root of time.

$$T_d = \frac{2q}{\sqrt{\pi}\sqrt{\lambda\rho c}} \sqrt{t} - \frac{d}{\lambda} q \qquad \text{(Eq. 8)}$$

Results and discussion

Validating the hypothesis (step 1)

The validity of the simplified approach shown in Fig. 1 would be validated if the surface temperatures plotted as a function of the square root of time $T_{surf} = f(\sqrt{t})$ showed the same linear behaviour as predicted by the simplified analytical Eq. 6. The natural heterogeneity of wood causes a certain variability of the experimental measurements of $T_{surf} = f(t)$ on the different replicate samples. Therefore, it is more reliable to validate the results of $T_{surf} = f(\sqrt{t})$ obtained by numerical simulation. Fig. 3 shows the results for beech in the early stages of heating (up to $3\sqrt{s}$). The table inserted in Fig. 3 summarises the corresponding results obtained for birch, Douglas-fir, and spruce. To keep in close touch with the reality of the experimental cases the values of the simulation parameters (rotation speed, s, flux density, q, and sample MC) and green log thermal parameters (thermal conductivity, λ, and specific heat capacity, ρc) were the same as those employed in the physical experiments (Table 1). From the results presented in Fig. 3, two conclusions can be drawn. Firstly, the linearity of the relationship $T_{surf} = f(\sqrt{t})$, confirmed by the high coefficients of determination, validates the assumption that the log can be treated as a semi-infinite body with a step increase in surface

temperature of a half-space. Secondly, for the four species, the near equivalence of α_{surf}^{simul} (calculated by linear regression analysis of numerical simulation curves) and $\alpha_{surf}^{anal} = \frac{2q}{\sqrt{\pi}\sqrt{\lambda\rho c}}$ (calculated by inserting the simulation parameters in Eq. 6) confirms the suitability of Eq. 6 for evaluating the surface temperature increment of a green rotating log under external IR heating based on the simplified approach. The slight difference between α_{surf}^{simul} and α_{surf}^{anal} in the case of spruce and Douglas-fir can be explained by the lack of linearity at the beginning of the curve (which is also visible in the other species) due to a perturbation at the early stages attributable to the numerical simulation.

Determining the effective RHFD, q, received by the sample (step 2)

From the results above, it is easy to estimate the effective RHFD, q, received by the sample by the inverse deconvolution method according to Beck et al. (1985). Here, the recorded surface temperature data, $T_{surf,}$, are the input to recover the signal q as it existed before it has been convolved by the impulse response of the half-space. The result of the deconvolution gives the maximum value (found to be around 10000 $W.m^{-2}$) of the estimated RHFD, q_{est}.

The deconvolution approach may be validated by measuring the spatial profile of the incident radiative heat flux received by the sample surface, q_{mes}, which corresponds directly to the electric signal produced by an IR sensitive sensor placed on the sample surface. For one sample, Fig. 4 compares the normalised values of the estimated heat flux density (HFD), q_{est}, with the measured IR sensor signal (which is proportional to the received HFD, q_{mes}) and shows a good agreement between estimation and measurement. This is also a confirmation of the results presented in the first paragraph, which were calculated by the Eqs. 6, 7, and 8, i.e. the temperature increase in a green log rotating under external IR heating can be described

reliably. Fig. 4 shows the spatial profile of the effective RHFD received by the sample which is the input data into the model for verification the simulation results.

Comparison of experimental and numerical simulation results (step 3)

In Figs.5 to 7, the residuals are calculated with the difference between experimental and modelled results and are plotted below each graph. Fig. 5a compares the surface temperatures $T_{surf} = f(t)$ of beech at 43% MC, obtained experimentally from surface thermocouples, with the numerical simulation results modelled with similar parameters (Table 1). Similar results were also obtained for birch at 85% MC (Fig. 5b), Douglas-fir at 115% MC (Fig. 5c), and spruce at 55% MC (Fig. 5d). In the 20 first seconds, the increasing slopes of the experimental curves are steeper than simulated (the residuals drop consequently below 0). This difference might be explained by some moisture gradients within the wood created during drying. These are responsible for the unavoidable heterogeneities in the thermal properties of wood. Moreover variations in the surface emissivities of different wood samples can lead to some errors in the HF received by the samples. But apart from this difference, these results show a good agreement between the numerical estimation and measurement (as can be seen by residuals which balance around 0). The comparison of temperatures $T_{3mm} = f(t)$ obtained experimentally with numerical simulation results is given for several replicates of birch at 85% MC (Fig. 6a), beech at 43% MC (Fig. 7a), Douglas-fir at 115% MC (Fig. 6b) and spruce at 55% MC (Fig. 7b). Regardless of the good results, around T_{max}, the residuals increase. This problem may arise from three side-effects: (1) The imprecise insertion depth of the thermocouples; the margin of error in the insertion depth of the thermocouples was estimated to be ±0.5mm, which clearly might have had an effect. (2) The effect of drying during heating; the difference in the block MC before and after heating, ΔMC_s, remained low (never exceeding 5%), however, even though it could not be reliably measured. This change

was attributed to water evaporating from the surface layers of the samples. (3) The influence of sawing; the differences in densities (and thus in thermal properties) between earlywood and latewood may have a greater influence in quarter sawn samples where annual rings are parallel to the IR flux. To take the effect of drying on thermal properties of wood into account, it is possible to estimate to 50% the margin of error on the MC. Assuming both effects (1) and (2), the envelope curves for the numerical simulation of $T_{3mm} = f(t)$ are plotted in Fig.7 (in dotted lines): in the most favourable case, where both insertion depth and MC are underestimated (Fig. 7a plots $T_{2.5mm} = f(t)$ at 21% MC and $T_{3.5mm} = f(t)$ at 65% MC for birch) and in the least favourable case when insertion depth and MC are overestimated (Fig. 7b plots $T_{2.5mm} = f(t)$ at 27% MC and $T_{3.5mm} = f(t)$ at 83% MC for spruce). When plotting these envelope curves, the effect of drying (2) dominates over the effect of the imprecise insertion of the thermocouples (1). The envelope curves surround all the experimental curves, which demonstrate that taking into account these two effects is more representative for the real experimental conditions.

Conclusion

By comparing experimental to numerical simulation results, this paper validates the ability of the numerical model developed by Dupleix et al. (2012a). The approach is based on finite elements to simulate two dimensional heat transfer within a log and to output the temporal evolution of surface temperatures and temperatures below the surface. The assumption concerning the applicability of the simplified approach turned out to be acceptable, and the simple analytical Eqs. 6 and 7 led to acceptable data. The inputs are the thermal and physical properties of green wood and the HFD of the infrared source. With the analytical equations provided in this article, it is possible to calculate rapidly (1) the maximum surface temperature reached by a green log with thermal characteristics, λ, and, ρc, rotating at a

peeling speed, s, under an IR heating source (HFD q, width x) and (2) the temperature at a certain depth below the surface. The heating rate that can be achieved is insufficient for most of today's industrial peeling speeds, but consideration should also be given to the fact that the use of an IR heating source obviates the need for lengthy soaking times and the associated infrastructure requirements, and so overall may be a worthwhile approach to log heating for veneer peeling.

Acknowledgements: This study was partly carried out in Aalto University (Finland), LaBoMaP-Arts et Metiers ParisTech Cluny (France) and I2M (France). The authors are thankful to these institutions for their support and to the RYM-TO Doctoral School for financial support.

References

Beck, J.V., St Clair, C.R., Blackwell, B. (1985) Inverse heat conduction. John Wiley and Sons Inc., New York

Bédard, N., Laganière, B. (2009) Debarking enhancement of frozen logs. Part II: infrared system for heating logs prior to debarking. Forest Prod. J., 59:25-30.

Braham-Bouchnak, T., Germain, G., Morel, A., Lebrun, J.L. (2013) The influence of laser assistance on the machinability of the titanium alloy Ti555-3. Int. J. Adv. Manuf. Techn., 68 (9-12):2471-2481.

Cserta, E., Hegedüs, G., Németh, R. (2012) Evolution of temperature and moisture profiles of wood exposed to infrared radiation. Bioresources, 7(4):5304-5311.

Coste, N. (2005) Interest of radiant energy for wood peeling and slicing processes. Master's thesis, Arts et Metiers ParisTech.

Dupleix, A., Marchal, R., Bléron, L., Rossi, F., Hughes, M. (2011) On-line heating temperatures of green-wood prior to peeling. Joint International Symposium on Wood Composites and Veneer Processing and Products Proceedings.

Dupleix, A., Ahmedou, S.A.O., Bléron, L., Rossi, F., Hughes, M. (2012a) Rational production of veneer by IR-heating of green wood during peeling: Modeling experiments. Holzforschung, 67(1):53-58.

Dupleix, A., Denaud, L., Bleron, L., Marchal, R., Hughes, M. (2012b) The effect of log heating temperature on the peeling process and veneer quality: beech, birch and spruce case studies. Eur. J. Wood Prod., 71(2):163-171.

Dupleix, A., De Sousa Meneses, D., Hughes, M., Marchal, R. (2012c) Mid infrared absorption properties of green wood. Wood Sci. Technol., 47(6):1231-1241

Dupleix, A., Kusiak, A., Hughes, M., Rossi, F. (2012d) Measuring the thermal properties of green wood by the transient plane source (TPS) technique. Holzforschung, 67(4): 437-445.

Grimhall, C.G., Hoel, O. (1983) Method of slicing veneer U.S. Patent No. 4,516,614. Filed June 3, 1983, and issued May 14, 1985.

Marchal, R., Gaudillière, C., Collet, R. (2004) Technical feasibility of an embedded wood heating device on the slicer or the peeling lathe. 1st International Symposium Veneer Processing and Products Proceedings, 29-44

Makoviny, I., Zemiar, J. (2004) Heating of wood surface layers by infrared and microwave radiation. Wood Research, 49(4):33-40.

Rahman Rashid, R.A., Sun S., Wang G., Dargusch M.S. (2012) The effect of laser power on the machinability of the Ti-6Cr-5Mo-5V-4Al beta titanium alloy during laser assisted machining. Int. J. Mach. Tool Manu., 63:41-43.

Suleiman, B.M., Larfeldt, J., Leckner, B., Gustavsson, M. (1999) Thermal conductivity and diffusivity of wood. Wood Sci. Technol., 33:465-473.

Taler, J., Duda P. (2006) Solving direct and inverse heat conduction problems. Springer, Berlin

Figure Captions

Figure 1 The experimental set-up for measuring the surface temperature of a rift sawn sample under IR heating.

Figure 2 Analogy of finite element model in 2D to semi-infinite behavior in 1D Cartesian coordinates.

Figure 3 Comparison of Finite Element simulated surface temperatures of rotating log and analytically calculated surface temperature response of half space. The temperatures are represented as a function of the square root of time for beech. Table: Comparison of numerical and analytical values of the slopes α_{surf}^{simul} and α_{surf}^{anal} of $T_{surf} = f(\sqrt{t})$ with their corresponding coefficients of determination, R^2, in the case of beech, birch, Douglas-fir and spruce.

Figure 4 Comparison of the estimated heat flux density and the measured IR sensor signal on one sample surface (normalised values are represented).

Figure 5 Comparison of numerical simulation curves of surface temperatures $T_{surf} = f(t)$ to experimental results obtained on different replicates of (a) beech at 43% MC, (b) birch at 85% MC, (c) Douglas-fir at 115% MC and (d) spruce at 55% MC (residuals are plotted below each graph).

Figure 6 Comparison of numerical simulation curves of temperatures measured at 3 mm depth $T_{3mm} = f(t)$ to experimental results obtained on different replicates of (a) birch at 85% MC, (b) Douglas-fir at 115% MC (residuals are plotted below each graph).

Figure 7 Comparison of experimental results measured at a depth of 3 mm with numerical simulation curves of temperatures $T_{3mm} = f(t)$ and their envelopes $T_{3\pm0.5mm} = f(t)$ (dotted lines) obtained on different replicates of (a) beech at 43±22% MC, (b) spruce at 55±28% MC (residuals are plotted below each graph).

Table Captions

Table 1 Thermophysical parameters and their corresponding values used in numerical and analytical simulations.

Figures

Fig1

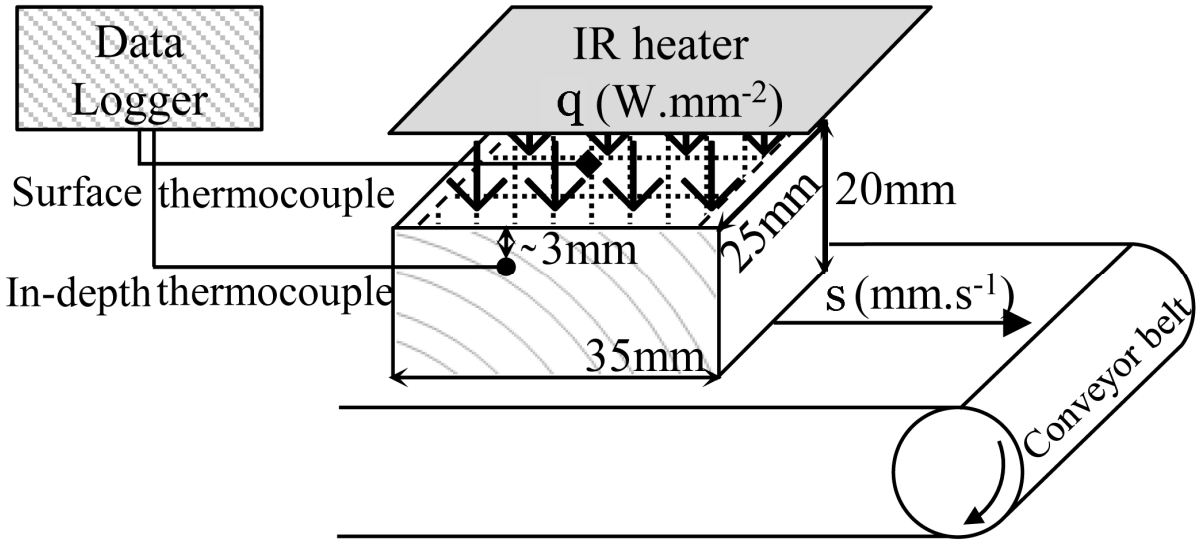

Fig2

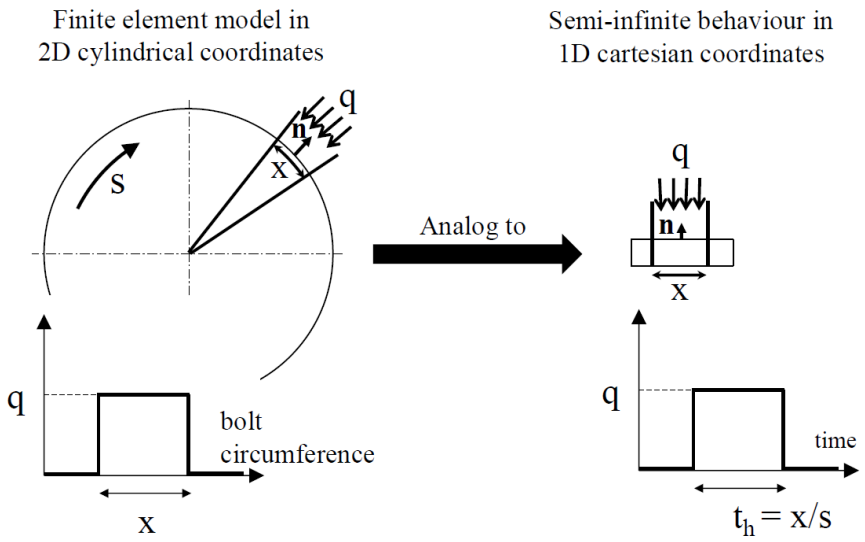

Fig3

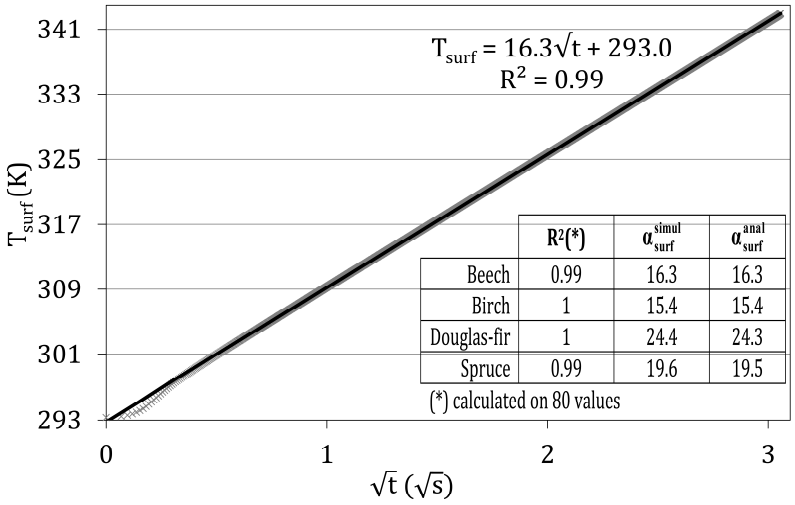

	R^2(*)	α_{surf}^{simul}	α_{surf}^{anal}
Beech	0.99	16.3	16.3
Birch	1	15.4	15.4
Douglas-fir	1	24.4	24.3
Spruce	0.99	19.6	19.5

Fig4

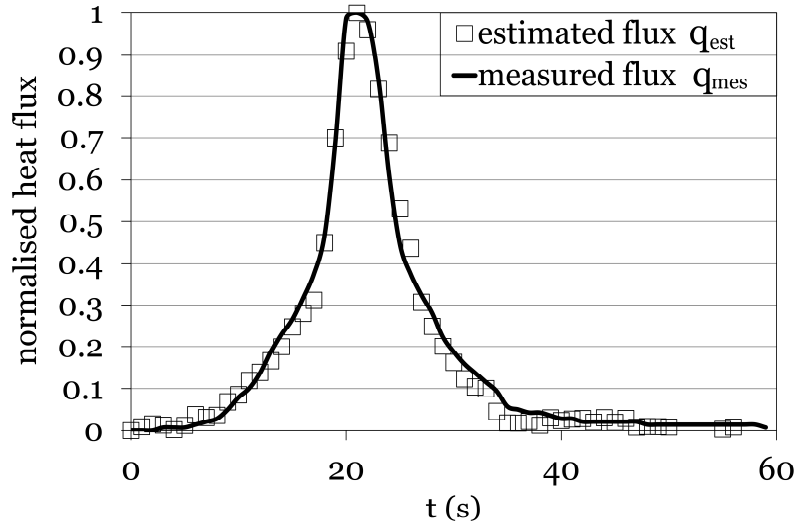

Fig5

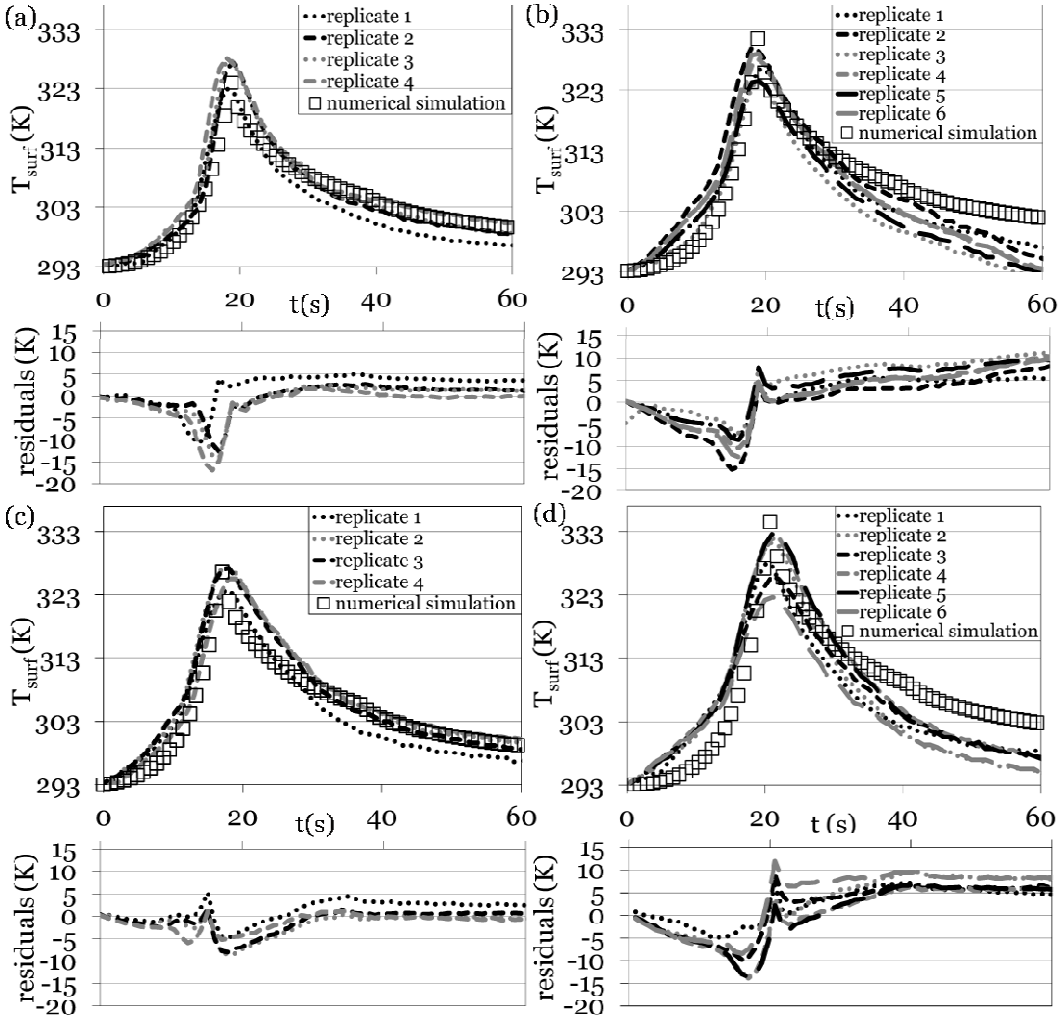
(a)
(b)
(c)
(d)
replicate 1
replicate 2
replicate 3
replicate 4
replicate 5
replicate 6
numerical simulation
T_{surf} (K)
residuals (K)
t(s)

Fig6

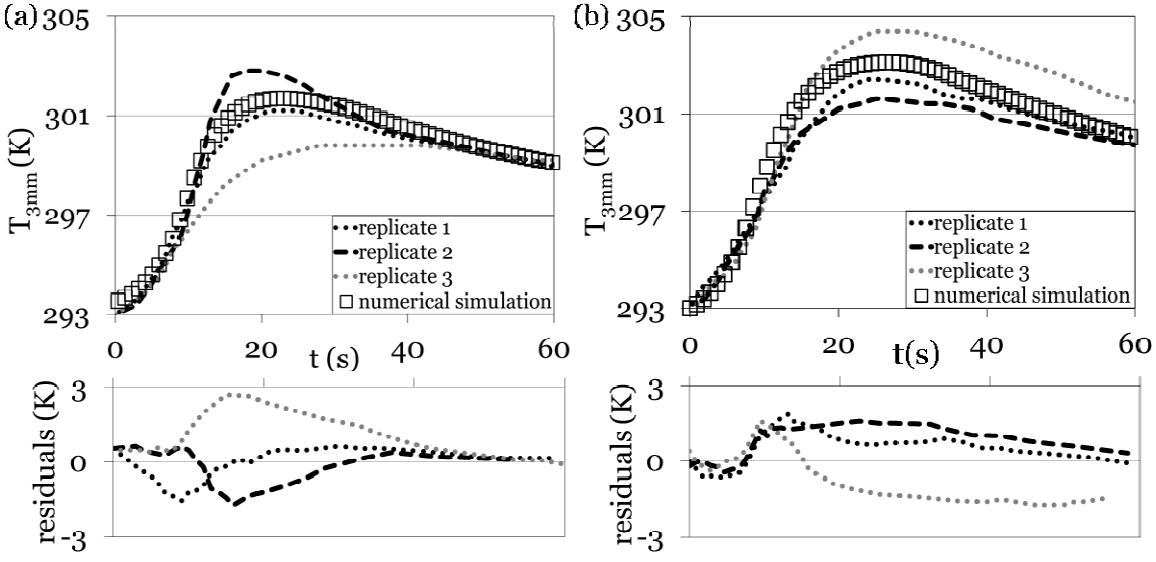
(a)
(b)
replicate 1
replicate 2
replicate 3
numerical simulation
T_{3mm} (K)
residuals (K)
t (s)
t(s)

Fig7

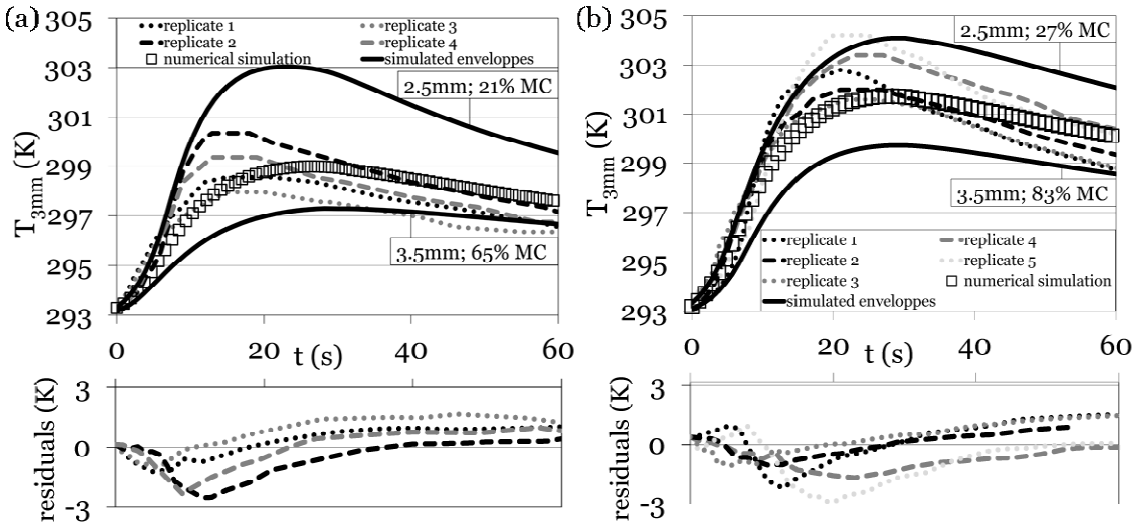

Tab1

(1) Dupleix et al. 2012d

Parameters	**Values**	
Rotating speed s ($m.s^{-1}$)	0.0032	
Density of flux q ($W.m^{-2}$)	10 000	
	Beech	**Birch**
Moisture Content MC (%)	43	85
Thermal conductivity λ ($W.m^{-1}.K^{-1}$)	0.30 (0.003MC+0.172) (1)	0.45 (0.003MC+0.191) (1)
Heat capacity ρc ($J.m^{-3}.K^{-1}$)	1.6E+06 (0.019MC+0.746)+06 (1)	1.2E+06 (0.021MC+0.577)+06 (1)
	Douglas-fir	**Spruce**
Moisture Content MC (%)	115	55
Thermal conductivity λ ($W.m^{-1}.K^{-1}$)	0.23 (1)	0.24 (0.002MC+0.130) (1)
Heat capacity ρc ($J.m^{-3}.K^{-1}$)	9.4E+05 (1)	1.4E+06 (0.032MC-0.311)+06 (1)